Contents lists available at ScienceDirect

Materials & Design

Microstructure and mechanical properties of friction spot welding aluminium–lithium 2A97 alloy

Chong Gao, Rongqiang Gao, Yue Ma [*]

Key Laboratory of Aerospace Materials and Performance (Ministry of Education), School of Materials Science and Engineering, Beihang University, Beijing 100191, China

A B S T R A C T

In this study, we investigated the microstructure and mechanical properties in different regions of the friction spot welded 2A97 aluminium–lithium alloy subjected to different heat treatment processes. The 2.0 mm thick hot-rolled sheet of 2A97 alloy was successfully welded using friction spot welding method with optimised welding parameters. Afterwards, the as-welded 2A97 joints experienced two subsequent heat treatment procedures: solution and ageing; directly ageing. The corresponding microstructure and mechanical properties of the heat-treated specimens were studied by means of optical microscope (OM), scanning electron microscope (SEM), transmission electron microscope (TEM), hardness test and tensile test. The results show that the mechanical properties of the 2A97 joints before and after heat treatment were significantly modified, which was mainly related to fine-grained microstructure, size and type of precipitates, and dislocation density. Compared to the base material and the material that only experienced direct ageing, the whole friction spot welded 2A97 joint after solution and ageing treatment delivered better mechanical properties.

© 2015 Elsevier Ltd. All rights reserved.

1. Introduction

The addition of lithium (Li) in aluminium (Al) alloy is beneficial to weight reduction of Al alloys. The density of Al alloys can be lowered by 3% as per 1 wt.% addition of Li. Al–Li alloys have experienced three generations since the first product of Al–Li alloy was developed in the 1920s. The previous two generations, such as 2020, 1420 and 8090, exhibited significant in-plane and through-thickness anisotropy in mechanical properties. That is the reason why the third generation of damage-tolerant products were developed [1–4]. The research work regarding Al–Li alloys provides potential for substantial weight saving in structural components due to their high strength and stiffness compared to conventional Al alloys. Al–Li 2A97 alloy is a type of innovative material, and the T8 treatment (artificially peak-aged) has been extensively applied in industry, especially in the aerospace industry [5,6].

Friction stir welding (FSW) is a solid state joining process invented by The Welding Institute (TWI) in UK, which is an effective welding method due to its low heat input and elimination of melting and solidification associated problems [7–9]. Friction stir

spot welding (FSSW) developed from friction stir welding (FSW) includes plunge and retraction processes of a composite tool [10]. Different from traditional resistance spot welding (RSW), FSSW is insensitive to materials and their surfaces. Furthermore, water, compressed air and electrical transforming equipment are not required for FSSW, leading to low investment and operating cost [11]. At present, there are three types of FSSW: friction spot welding (FSpW), plunge FSSW and swing FSSW [12]. FSpW offers more advantages over conventional spot joining techniques, such as high energy efficiency and surface quality, environmental compatibility and improved performance [11,13–15]. FSpW is also used to fill the pullout holes resulting from FSW [16], fabricate skin stiffened panel [17] and repair fatigue crack [18]. FSpW can be divided into pin-plunge and sleeve-plunge [19] depending on plunging components. Sleeve-plunge FSpW was used in this study due to the formation of large weld zone and the acquirement of the joint with superior shear strength [20].

So far, some Al alloy joints have been produced by FSpW. The microstructure and corresponding mechanical properties of the joints have been investigated. For instance, Sergio et al. [20] studied the effects of rotational speed and joining duration on the strength of AA 2024-T3 overlap welds produced by FSpW. Shen et al. [10] investigated the microstructure and mechanical properties of FSpW 7075-T6 Al alloy joint, and discussed the generation of defects and the failure mechanisms. However, little research work

---

[*] Corresponding author.
  E-mail address: mayue@buaa.edu.cn (Y. Ma).

regarding the FSpW of Al–Li alloy is available in the public domain. In recent years, with the rapid development of FSpW, it is increasingly applied for Al–Li alloy. Thus it is imperative to investigate and clarify the microstructure and properties of Al–Li alloy joints produced by FSpW.

This research focused on the local microstructure and mechanical properties of the friction stir spot welded Al–Li 2A97 alloy. In order to improve the mechanical properties of the joint, different heat treatment processes were designed and performed for the joint. The microstructure of as-deposited and postweld heat-treated specimens were characterised using optical microscope (OM), transmission electron microscope (TEM), scanning electron microscope (SEM) and energy dispersive spectroscopy (EDS). Furthermore, the corresponding tensile strength and hardness of the joints were performed to evaluate the effects of heat treatment on microstructure and mechanical properties.

2. Experimental work

The material used in this study was 2.0 mm thick hot rolled Al–Li 2A97 sheet supplied by Aluminum Corporation of China. The chemical composition of as-received Al–Li 2A97 alloy is listed in Table 1, and the FSpW process was conducted on the FSpW equipment provided by Beijing Aeronautical Manufacturing Technology Research Institute, China. The key parameters of the FSpW process were: the rotational speed, 1000 rpm; the dwell time, 2 s. A composite tool used in this study had a shoulder with diameter of 9.0 mm and a pin with diameter of 6.0 mm. The macroscopic image of the friction spot welded surface of the hot rolled 2A97 sheet is shown in Fig. 1.

To investigate the effects of subsequent heat treatment on the microstructure and mechanical properties, the friction spot welded 2A97 (FSpW 2A97) specimens were subjected to two designed heat treatment processes (Table 2). The HT1 process consisted of solution treatment at 520 °C for 2 h, quenching in water and ageing at 175 °C for 12 h. It was reported that peak hardness of Al–Li alloys may be achieved under HT1 condition [21–23]. By contrast, during the HT2 process the FSpW 2A97 specimens were only aged at 175 °C for 12 h without any solution treatment. HT2 was designed to compare with HT1 since the highest temperature during FSpW is 0.7–0.9 T_m (T_m: melting temperature of material) [24].

The as-deposited and postweld heat-treated specimens were cut through the cross-sections and prepared according to the standard metallographic procedures. After etching in Keller's solution (2 ml HF + 3 ml HCl + 5 ml HNO_3 + 190 ml H_2O) for 15 s, the microstructure of the specimens was analysed using Leica DFC295 OM. To observe the precipitates in the specimens on JEM 2100F TEM, thin foils were twin-jetted in the electrolyte of 25 vol.% nitric acid and 75 vol.% methanol. To characterise the precipitation, the thin foils were observed using JEM 2100F TEM. Atomic concentrations of the precipitates were also measured by EDS detector attached to TEM.

According to ASTM E384-11e1 and ASTM E8/E8M-13a, Vickers hardness (HV) testing was performed using the load of 200 g and dwell time of 15 s on HXZ-1000 hardness tester, and tensile testing was performed at room temperature with strain rate of 6.7×10^{-3} s^{-1} on Instron-8801 tensile tester. The values of hardness, ultimate tensile strength (UTS), yield strength (YS, 0.2% proof stress) and elongation (δ) were recorded. Fig. 2 displays the

Table 1
Chemical composition (wt.%) of the studied Al–Li 2A97 alloy.

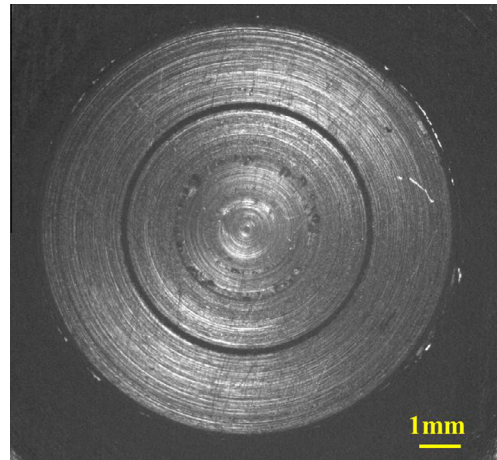| Cu	Li	Mg	Zn	Mn	Zr	Al
4.0	1.4	0.4	0.5	0.3	0.1	Bal.

Fig. 1. Macroscopic image of the friction spot welded surface of the hot-rolled 2A97 sheet.

Table 2
Two different heat treatment processes of the FSpW 2A97 joint.

Sample No.	Process	Solution treatment	Ageing
FSpW-HT1	HT1	520 °C/2 h	175 °C/12 h
FSpW-HT2	HT2	–	175 °C/12 h

schematic illustration of the mechanical testing. After tensile testing, the fracture morphologies of the specimens were observed using CS-3400 SEM.

3. Results and discussion

3.1. Microstructure analyses

3.1.1. Microstructure of the FSpW 2A97 joint

The longitudinal section macrograph of the welded specimen with a plunge depth of 1.5 mm is displayed in Fig. 3. It is evident that a high-quality joint was successfully produced using the selected welding parameters. The weld profile appears a "basin" shape, which can be divided into three regions: the stir zone (SZ), the thermo-mechanically affected zone (TMAZ) and the heat-affected zone (HAZ). In addition, the SZ region consists of the stir shoulder zone (SsZ) and the stir pin zone (SpZ).

Optical micrographs of the different regions of the FSpW 2A97 joint are illustrated in Fig. 4. For a 2.0 mm thick hot-rolled 2A97 sheet, BM exhibited typical hot-banded microstructure parallel to the rolling direction (Fig. 4a). The microstructure of HAZ was similar to that of BM due to limited temperature during the welding process (Fig. 4b). In TMAZ, a distorted structure with re-oriented grains formed (Fig. 4c) due to the combined effects of shear stress and heat diffusion caused by the driving force of the tool. In SsZ (Fig. 4d) and SpZ (Fig. 4e), banded microstructure disappeared and homogeneous microstructure appeared. In these two regions, the combination of shear stress, heat diffusion and resulted higher temperature leads to homogeneous microstructure.

The precipitates in the different regions of the FSpW 2A97 joint were characterised by both bright field (BF) image and selected area electron diffraction (SAED) pattern viewed along $[\bar{1}11]_{Al}$ axis or $[\bar{1}12]_{Al}$ axis. It can be observed from the SAED patterns that only Al matrix diffraction spots existed in the FSpW joint, indicating that no strengthening phases precipitated in Al matrix. The evolution of grain shape and size of the joint are displayed in the BF images (Fig. 5). In BM a small amount of sub-grains formed

(Fig. 5a), while in HAZ some substructures grew into fine grains (Fig. 5b). More fine grains (approximately 0.6 μm) formed in TMAZ (Fig. 5c) due to the heat diffusion and shear stress. It is well known that both the plastic deformation and frictional heat influenced SsZ and SpZ during FSpW. As mentioned before, more homogeneous microstructure was found in the SZ region. It should be noted that in SsZ (Fig. 5d) the elongated grains with size of 1.2 ± 0.6 μm were found, whereas in SpZ (Fig. 5e) the equiaxed grains with size of 0.6 ± 0.5 μm were observed. The formation of refined grains in the weld centre was attributed to recrystallisation and thermally activated high angle grain boundary migration. The grains can grow as the temperature goes up towards the tool [13,25,26]. In HAZ, fine grains formed due to the thermal diffusion below the recrystallisation temperature of Al–Li alloy [25,27].

While a small amount of dispersed rod- and spherical-shaped particles, which could not be detected through SAED, were observed in the BF images. The rod-shaped Mn-rich precipitates (Fig. 6a) were identified as $Al_{20}Cu_2Mn_3$, and the spherical-shaped Zr-rich precipitates (Fig. 6b) were judged to be β′ (Al_3Zr) [28–30]. It is published [31] that the dispersed phases of $Al_{20}Cu_2Mn_3$ and β′ (Al_3Zr) mainly determine the size of recrystallised grains.

3.1.2. Microstructure of the FSpW 2A97 after HT1

After HT1 (solution and ageing treatment), it is evident from the TEM images that a large amount of fine grains formed in the banded grains of BM (Fig. 7a). However, in SpZ, the grains significantly grew up, even larger than 300 μm (Fig. 7b).
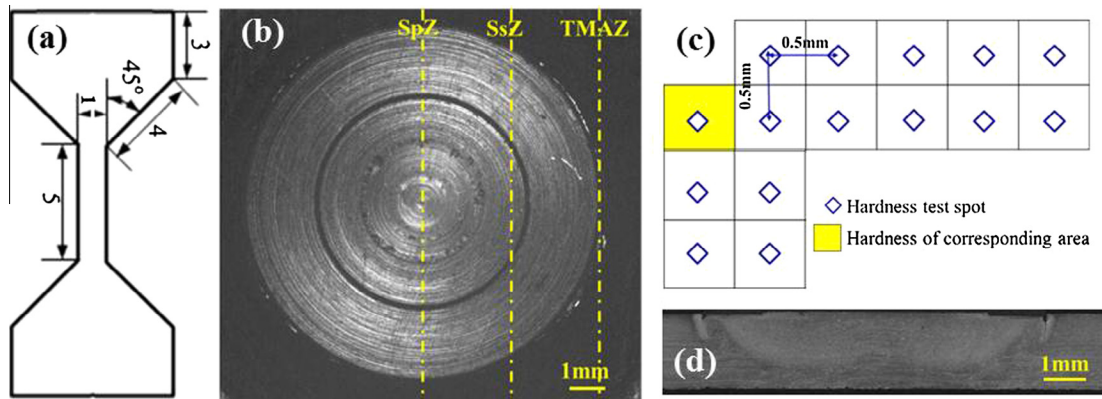

Fig. 2. Schematic illustration of the mechanical testing of the hot-rolled Al–Li 2A97 sheet: (a) size of tensile specimen; (b) locations of tensile specimens (dash lines are located in the middle of tensile specimens); (c) locations of hardness indentation; (d) longitudinal section for hardness testing.
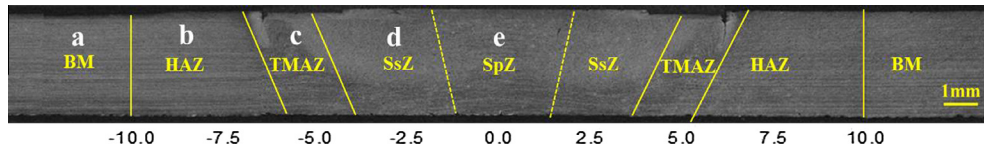

Fig. 3. Optical macrograph of the longitudinal section of FSpW 2A97 Al–Li alloy.
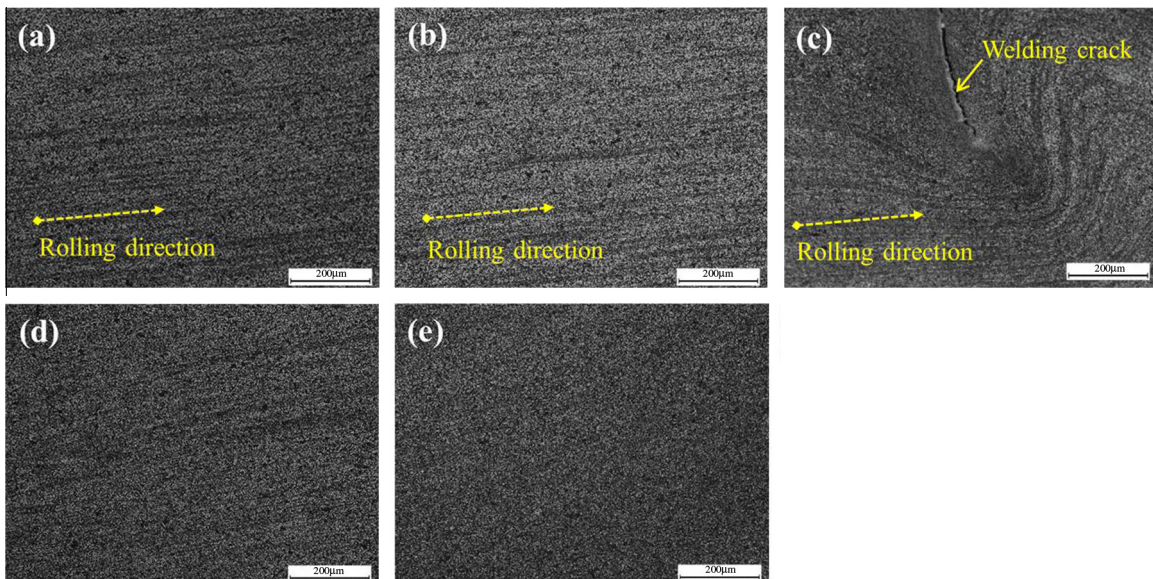

Fig. 4. Optical micrographs of the FSpW 2A97: (a) BM; (b) HAZ; (c) TMAZ; (d) SsZ; (e) SpZ.

Fig. 8 displays the TEM images of the BM and SpZ regions. From the SAED patterns (Fig. 8a and c), three sets of diffraction spots were found, including Al matrix diffraction spots. The super lattice spots (blue rhombus) were from β' (Al_3Zr) phase or δ' (Al_3Li) phase [32,33]. In the BF images (Fig. 8b and d) some dispersed β' (Al_3Zr) and δ' (Al_3Li) phases were observed, both of which were spherical-shaped. However, one can differentiate between these two phases from the EDS results: β' (Al_3Zr) phase contains Zr element whereas δ' (Al_3Li) phase does not contain Zr element. The diffraction spots at 1/3 $[\bar{1}\bar{1}0]_{Al}$ (yellow hexagon) were from the T1 phases (crystallographic structure: hexagonal, $a = 0.496$ nm, $c = 0.935$ nm; space group: P6/mmm; orientation relationship: $(0001)_{T1}//(111)_{Al}$, $[2\bar{1}\bar{1}0]_{T1}//[\bar{1}12]_{Al}$; habit plane: $\{111\}$) [1,34]. However, in the BF image of BM (Fig. 8b), a large amount of needle-shaped T1 phases, with length of 122.5 ± 50.5 nm, was located on the $(111)_{Al}$ plane. In the BF image
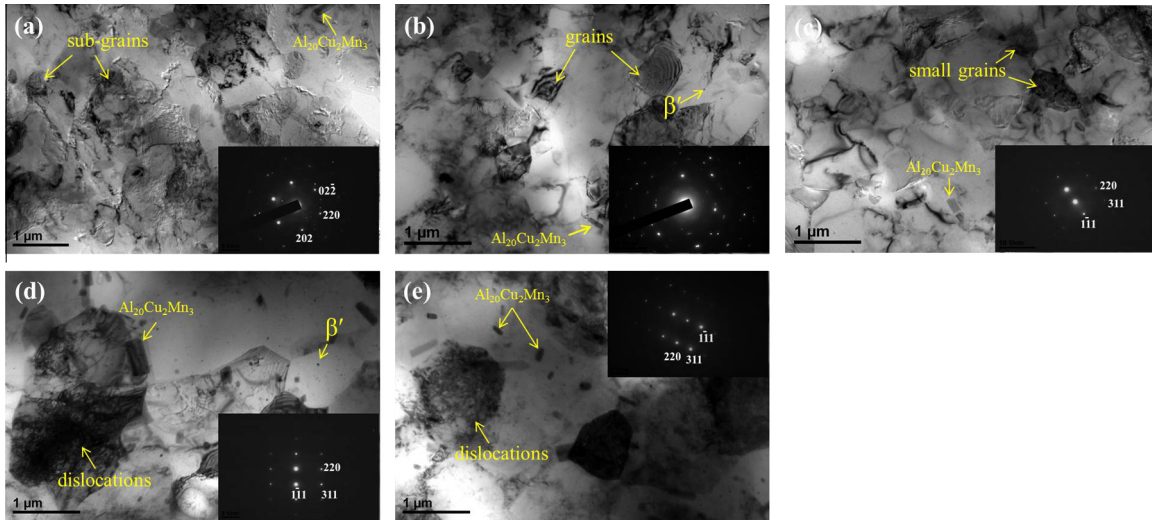

Fig. 5. TEM images (BF image and SAED pattern) of the different regions of the FSpW 2A97: (a) BM; (b) HAZ; (c) TMAZ; (d) SsZ; (e) SpZ.
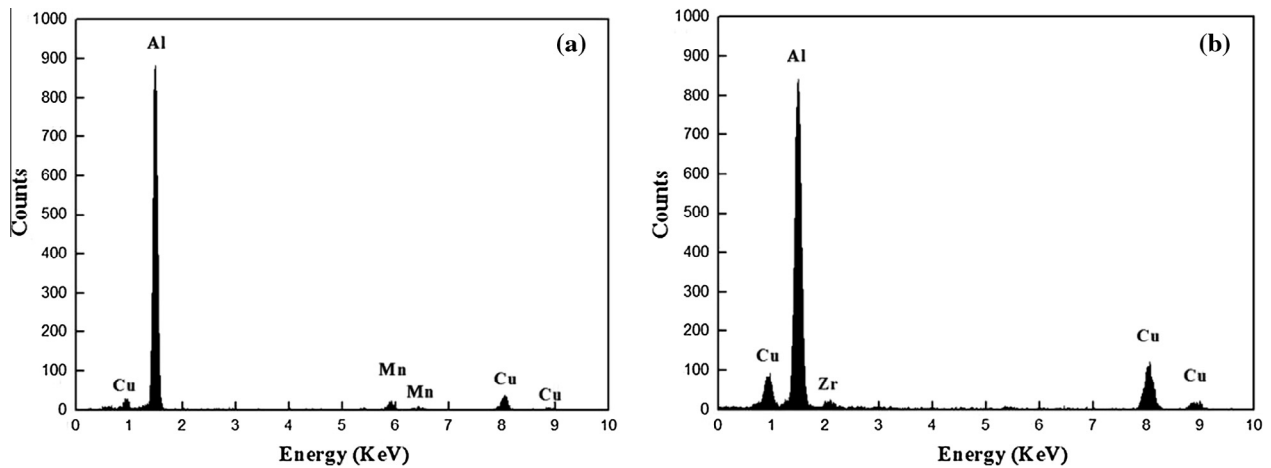

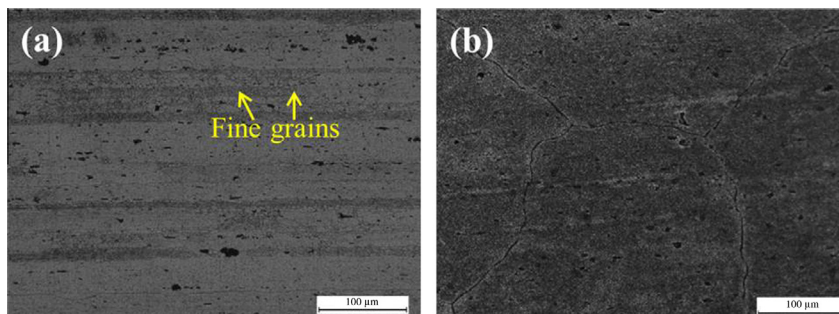**Fig. 6.** EDS analyses: (a) rod-shaped particle; (b) spherical-shaped particle.

Fig. 7. Optical micrographs of FSpW-HT1: (a) BM; (b) SpZ.

of SpZ region (Fig. 8d), the number density of needle-shaped T1 phases slightly increased, and the length decreased to 113.1 ± 56.4 nm. In addition, S′ (Al$_2$CuMg) phase with size of around 200 nm was observed to be parallel to the $(2\,4\,0)_{Al}$ plane [35].

Lin et al. [36] studied the influences of ageing treatment on Al–Li 2A97 alloy and recognised that the highest strength could be achieved after ageing for the hot-rolled 2A97 alloy. A mass of fine dispersed T1 phase and a small quantity of S′ (Al$_2$CuMg) phase within the grains contributed to the high strength. Li et al. [6] stated that the appropriate pre-deformation in the 2A97 sheet was beneficial to the increase of dislocation density, which was able to provide more nucleation sites for θ′ and T1 phases. In this study, after the solution and ageing treatments, no S′ phase was observed in BM, which indicated that BM was at underaged condition. But after severe plastic deformation through FSpW, more nucleation sites generated in SpZ, which promoted the formation of T1 and S′ phases, and ultimately delivered the highest strength for the FSpW 2A97 joint.

3.1.3. Microstructure of the FSpW 2A97 after HT2

Microstructure in BM and SpZ of the FSpW 2A97 after HT2 (directly ageing) are shown in Fig. 9. Compared to HT1, no distinct change in grain size was found after ageing treatment, but the banded microstructure disappeared in BM. Meanwhile, most of the recrystallised grains remained unchanged after HT2 in SpZ.

The precipitation in SpZ of the FSpW 2A97 joint was also examined using TEM. Three sets of diffraction spots indicated that T1, δ′ and β′ phases formed in this region. From the BF image shown in Fig. 10b, the length of needle-shaped T1 precipitates on $\{1\,1\,1\}_{Al}$ planes ranged from 200 to 300 nm. It is evident that the amount of T1 phase was related to the absence of solution treatment. Without solution treatment, the element of Li was not uniformly distributed in the Al matrix and the free energy for T1 precipitation was insufficient. In spite of more nucleation sites generated after FSpW, T1 phases could not precipitate in a great number during the HT2 process.

3.2. Hardness distribution

The 2D microhardness map of the longitudinal section of the as-deposited FSpW 2A97 joint is shown in Fig. 11a. The hardness distribution profile exhibited a symmetrical "basin" shape, matching well with the microstructure. The hardness values of BM and SpZ were similar (approximately 90 HV$_{0.2}$). In SsZ, the hardness increased to about 115 HV$_{0.2}$. On contrast, in TMAZ, the hardness
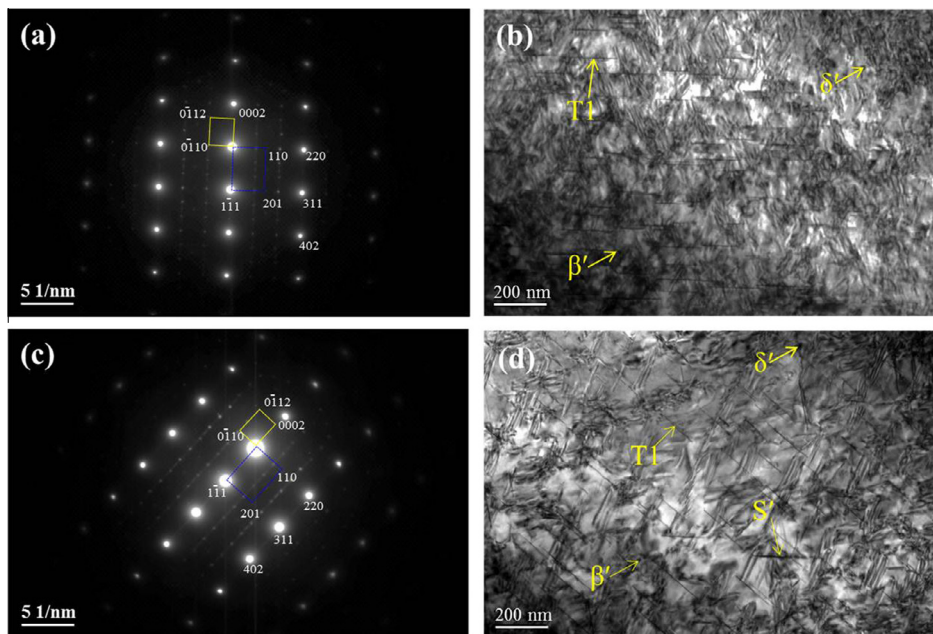

Fig. 8. TEM images of FSpW-HT1 viewed along $[\bar{1}\,1\,2]_{Al}$ axis: (a) SAED pattern in BM; (b) BF image in BM; (c) SAED pattern in SpZ; (d) BF image in SpZ.
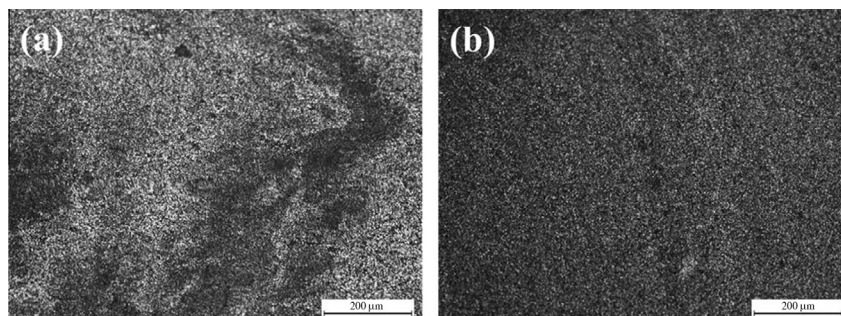

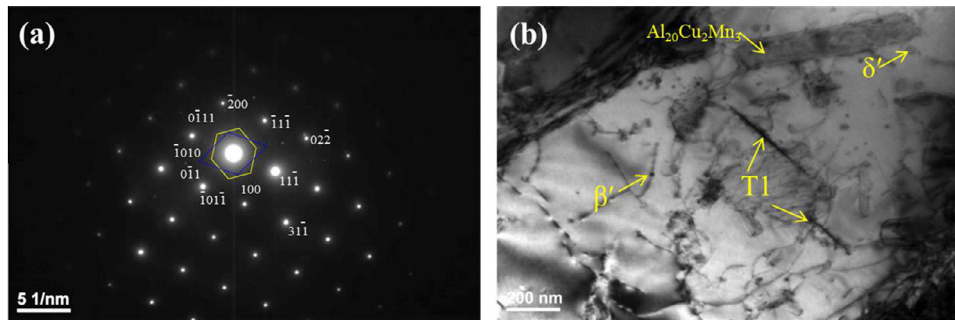**Fig. 9.** Optical micrographs of FSpW-HT2: (a) BM; (b) SpZ.

Fig. 10. TEM images in SpZ region of FSpW-HT2 viewed along [0 1 1]$_{Al}$ axis: (a) SAED pattern; (b) BF image.
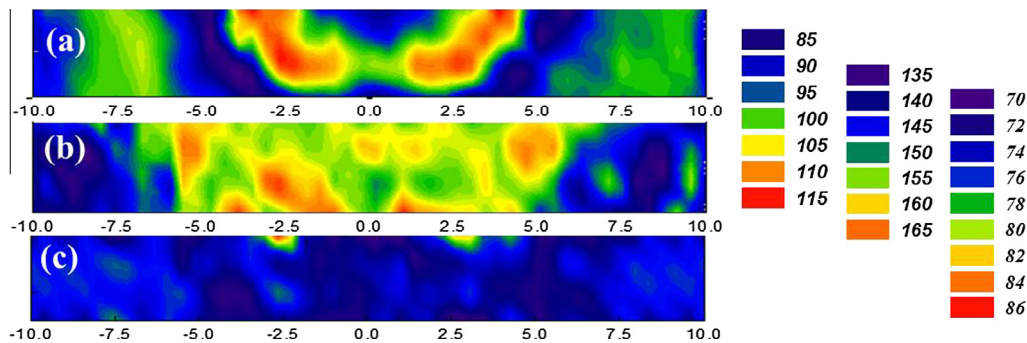

Fig. 11. Hardness distributions of: (a) FSpW 2A97; (b) FSpW-HT1; (c) FSpW-HT2.

decreased to 90 HV$_{0.2}$. Meanwhile, the hardness of HAZ varied in the range of 85–100 HV$_{0.2}$.

Fig. 11b displays the hardness distribution of FSpW-HT1. It is apparent that the hardness values also distributed as a "basin" shape. The hardness of SpZ was around 20 HV$_{0.2}$ higher than that of BM. Compared to the hardness before heat treatment, the average hardness of BM and SpZ increased by 50 HV$_{0.2}$ and 45 HV$_{0.2}$, respectively.

Fig. 11c shows the hardness distribution of FSpW-HT2. It can be seen that the "basin" shape profile disappeared. The hardness in SpZ and BM regions was at the same level (around 80 HV$_{0.2}$).

Shen et al. [10,12] investigated the hardness distribution on the surfaces of the FSpW 6061 and 7075 alloys and found that the weldment exhibited inverted sawtooth shape, which was related to the grain size and precipitation. In this study, the hardness distribution was associated with grain size, dislocation density and precipitation. Before heat treatment, as no T1 phase was observed in the FSpW 2A97 joint, the hardness of the different regions was dependent on grain size and dislocation density. Theoretically, the higher hardness was related to finer grain size and higher dislocation density. After HT1, the hardness dramatically increased to 160 HV$_{0.2}$ as a result of a large amount of fine T1 phases. It is interesting to found that the grain coarsening (>300 μm) occurred in SpZ region did not lead to low hardness. This is though to be associated with the formation of significant numbers of precipitates, which can offset the negative influence of coarse grain on hardness. After HT2, the hardness of different regions of the FSpW 2A97 joint apparently decreased in SpZ region since a few dislocation tangles were retained in grains. Despite the finer recrystallised grains in SsZ, no difference of hardness between BM and SpZ was found. This indicated that the grain size had less influence on the hardness than dislocation density. Hence, it is quite reasonable to conclude that for Al–Li 2A97 alloy the hardness is firstly related to precipitation size and type, followed by dislocation density and then grain size.
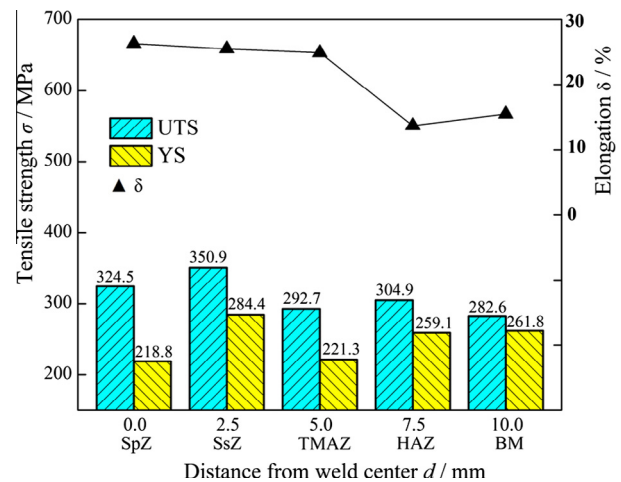

Fig. 12. Tensile strength of the different regions of the FSpW 2A97.

3.3. Tensile strength

Fig. 12 displays the tensile properties of the different regions of the as-deposited FSpW 2A97 joint. It is apparent that compared to the elongation of BM (15.5%) and HAZ (13.7%), the elongation of the other regions were apparently improved, i.e. 26.3% for SpZ, 25.5% for SsZ, and 24.9% for TMAZ. The YS in the different regions exhibited a linear relationship with the hardness. The YS (σ_y) can be converted to the hardness (HV) via a simple regression equation [37]. Eq. (1) applies to age hardening Al–Li 2A97 alloys and is valid for the FSpW 2A97 joint in this study.

$$HV = 0.33\sigma_y + 16.0 \tag{1}$$

Compared to BM, the value of UTS was improved after the FSpW process. The UTS in SsZ and SpZ reached 350.9 MPa and 324.5 MPa, which increased by 24.2% and 14.8%, respectively. Meanwhile, the
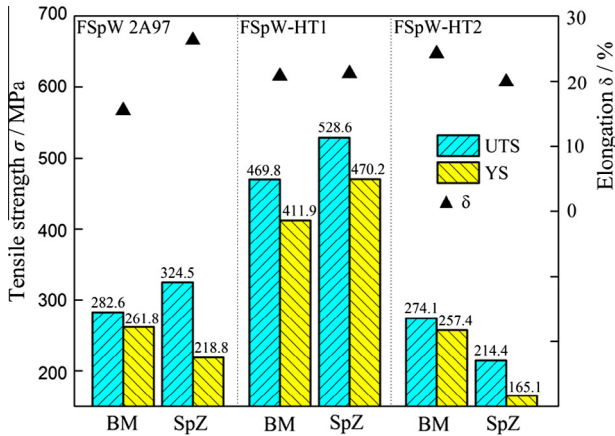
Fig. 13. Tensile strength in BM and SpZ of the FSpW 2A97 joint after HT1 and HT2.

elongation in SsZ and SpZ was improved by 64.5% and 69.7%. Fine recrystallised grains formed in these two regions (Fig. 5d and e). Under tensile deformation, slip motion occurred and grain boundaries acted as an impediment to dislocation motion [38], leading to higher stress before failure.

Compared to BM, the UTS in TMAZ (292.7 MPa) and HAZ (304.9 MPa) were slightly increased. The presence of welding crack

in TMAZ (Fig. 5c) was likely to be detrimental to the final mechanical properties. In HAZ (Fig. 5b), some sub-grains grew up to fine equiaxed grains due to heat diffusion, delivering a relatively higher tensile strength.

Fig. 13 shows the tensile properties of BM and SpZ of the FSpW 2A97 specimen after HT1 and HT2. It can be seen that compared to the as-deposited FSpW 2A97 specimen, the elongation of BM increased from 15.5% to 20.8% for specimen after HT1 and to 24.2% for specimen after HT2, respectively. The elongation of SpZ after HT1 decreased from 26.3% to 21.2% and to 19.9% after HT2. It is apparent that the tensile strength was influenced by heat treatment. Compared to the original FSpW 2A97, after HT1 the UTS values of BM and SpZ increased to 469.8 MPa and 528.6 MPa, respectively. On the contrary, after HT2 the UTS of BM and SpZ decrease by 8.5 MPa and 110.1 MPa respectively compared to the original FSpW 2A97 specimen.

After HT1, the grain size in SpZ grew up to larger than 300 μm. A large number of T1 and some S′ (Al_2CuMg) phases precipitated. It has been well known that stable T1 phase formed on $(1 1 1)_{Al}$ plane was considered as the main strengthening phase in Al–Li alloys [34,39–41]. The nucleation sites of T1 phase was strongly dependent on the application of plastic deformation prior to ageing, involving abundant dislocations in the Al matrix [34,42,43], which resulted in the improvement of the UTS from 324.5 MPa to 528.6 MPa. It was reported that the Al–Li 2A97 alloy was processed through thermo-mechanical treatment, the UTS value of the 2A97
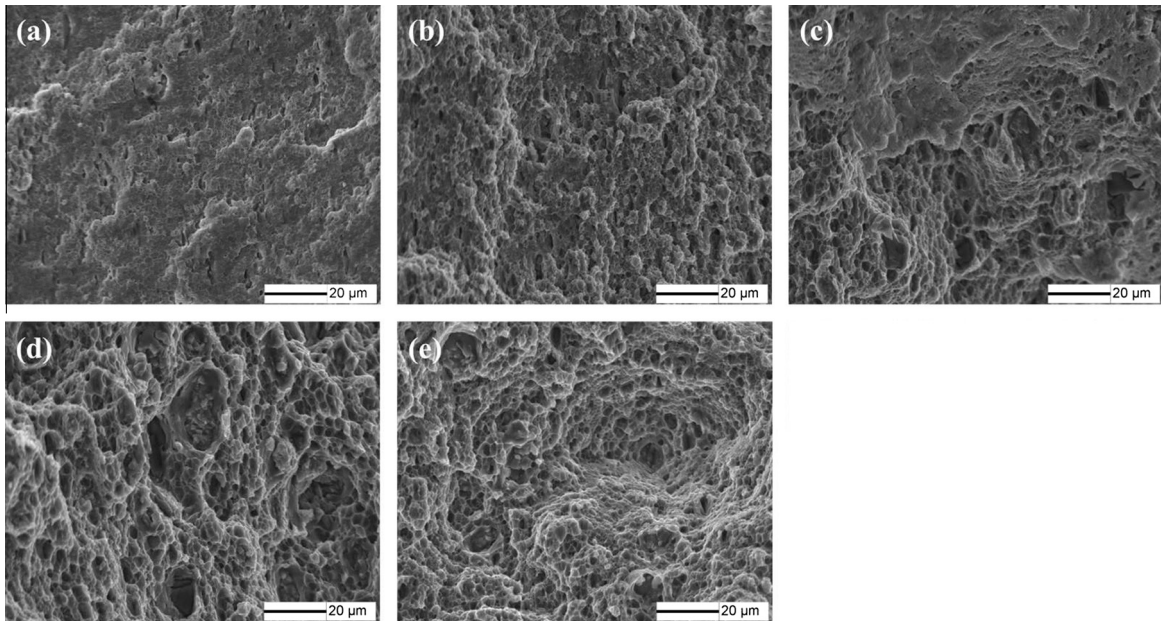

Fig. 14. Fracture surfaces in the different regions of the FSpW 2A97 specimens: (a) BM; (b) HAZ; (c) TMAZ; (d) SsZ; (e) SpZ.
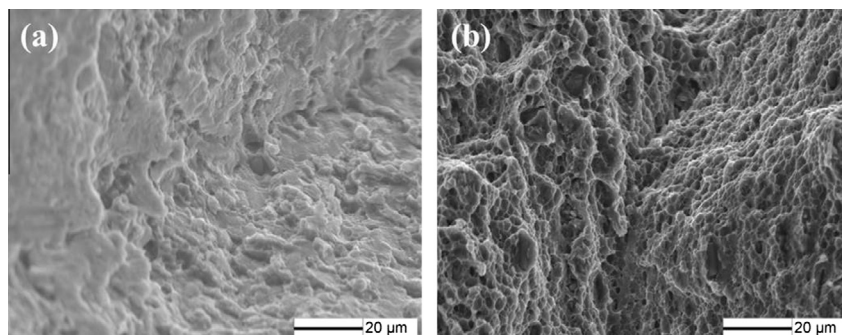

Fig. 15. Fracture surfaces in SpZ of the FSpW 2A97 specimens: (a) FSpW-HT1; (f) FSpW-HT2.

alloys increased to 534.3 MPa, which was related to a large amount of tiny T1 and a few S′ precipitates [23]. This demonstrated that the HT1 heat treatment after FSpW had the same effect on properties as that of the thermo-mechanical treatment.

The UTS in BM and SpZ decreased after HT2 since a small amount of coarse T1 phase re-precipitated, which indicated that the combination of shear stress and frictional heat during FSpW was not able to be the substitute for solution treatment for Al–Li alloy.

3.4. Fracture surface analyse

Fig. 14 shows the fracture surfaces of the different regions of the FSpW 2A97 specimens under SEM after tensile testing. It can be seen from Fig. 14a that the fracture morphology of BM exhibited flat facets and shallow dimples. In HAZ (Fig. 14b), a large amount of dimples increasingly appeared. In TMAZ, the size of dimples became further larger (Fig. 14c); while in SsZ (Fig. 14d) and SpZ (Fig. 14e), the number of dimples increased and the size became smaller, which was beneficial to the mechanical properties. It is acceptable that the fracture modes were ductile for all regions of the FSpW 2A97 joint.

After HT1, as shown in Fig. 15a, the mixed facture of shallow dimples and flat facets appeared in the surface of SpZ. By contrast, the deeper and larger dimples, together with a small amount of flat facets, were observed in the surface of SpZ after HT2 (Fig. 15b). Although both surfaces retained comparatively good ductility based on the results of elongation, the ductility was worse after both heat treatment procedures.

4. Conclusion

In the present study, the microstructure and mechanical properties of a 2.0 mm friction spot welded 2A97 Al–Li hot rolled sheets were investigated. The high-quality welds were successfully produced by using a composite tool and selected welding parameters. The following conclusions can be drawn:

(1) During the FSpW process, and the original banded grains in 2A97 Al–Li alloy were transformed to fine equiaxed grains. The hardness distribution exhibited a "basin" shape, which was related to the size and type of precipitates, dislocation density and grain size. Compared to BM, the UTS values of SsZ and SpZ regions were apparently increased due to the fine recrystallised grains.

(2) After the HT1 treatment (solution and ageing), the UTS values of SpZ increased due to a large amount of T1 phase and some S′ (Al_2CuMg) phase. The coarse grains in SpZ did not significantly influence the strength and hardness. However, after the HT2 treatment (directly ageing), a small number of coarse T1 phase and only a few tangled dislocations were observed, leading to the reduction of tensile strength and hardness.

(3) The fractography of SpZ after HT1 and HT2 changed from all dimple fracture into a mixed fracture, which suggested that the subsequent heat treatment could deteriorate the ductility of 2A97 Al–Li alloy.

References

[1] B. Decreus, A. Deschamps, F. De Geuser, P. Donnadieu, C. Sigli, M. Weyland, The influence of Cu/Li ratio on precipitation in Al–Cu–Li−x alloys, Acta Mater. 61 (2013) 2207–2218.

[2] T. Dursun, C. Soutis, Recent developments in advanced aircraft aluminium alloys, Mater. Des. 56 (2014) 862–871.

[3] J.F. Li, Z.Q. Zheng, Y.L. Chen, X.H. Zhang, Al–Li alloys and their application in aerospace industry, Aerospace Mater. Technol. 42 (2012) 13–19.

[4] R.J. Rioja, J. Liu, The evolution of Al–Li base products for aerospace and space applications, Metall. Mater. Trans. A 43 (2012) 3325–3337.

[5] A. Deschamps, B. Decreus, F. De Geuser, T. Dorin, M. Weyland, The influence of precipitation on plastic deformation of Al–Cu–Li alloys, Acta Mater. 61 (2013) 4010–4021.

[6] H.Y. Li, X.F. Wang, J. Bin, D.D. Wei, J.F. Zhang, Effect of two aging processes on microstructure and properties of alloy 2A97, J. Cent. South. Univ. (2011) 1261–1269.

[7] J. Han, H.J. Li, Z.X. Zhu, F. Barbaro, L.Z. Jiang, H.G. Xu, et al., Microstructure and mechanical properties of friction stir welded 18Cr–2Mo ferritic stainless steel thick plate, Mater. Des. 63 (2014) 238–246.

[8] R.S. Mishra, Z.Y. Ma, Friction stir welding and processing, Mater. Sci. Eng., R 50 (2005) 1–78.

[9] R. Rai, A. De, H. Bhadeshia, T. DebRoy, Review: friction stir welding tools, Sci. Technol. Weld. Join. 16 (2011) 325–342.

[10] Z. Shen, X. Yang, Z. Zhang, L. Cui, T. Li, Microstructure and failure mechanisms of refill friction stir spot welded 7075–T6 aluminum alloy joints, Mater. Des. 44 (2013) 476–486.

[11] Y. Uematsu, K. Tokaji, Y. Tozaki, T. Kurita, S. Murata, Effect of re-filling probe hole on tensile failure and fatigue behaviour of friction stir spot welded joints in Al–Mg–Si alloy, Int. J. Fatigue 30 (2008) 1956–1966.

[12] Z. Shen, X. Yang, S. Yang, Z. Zhang, Y. Yin, Microstructure and mechanical properties of friction spot welded 6061–T4 aluminum alloy, Mater. Des. 54 (2014) 766–778.

[13] P. Fanelli, F. Vivio, V. Vullo, Experimental and numerical characterization of Friction Stir Spot Welded joints, Eng. Fract. Mech. 81 (2012) 17–25.

[14] Y. Tozaki, Y. Uematsu, K. Tokaji, A newly developed tool without probe for friction stir spot welding and its performance, J. Mater. Process. Tech. 210 (2010) 844–851.

[15] W. Yuan, R.S. Mishra, B. Carlson, R. Verma, R.K. Mishra, Material flow and microstructural evolution during friction stir spot welding of AZ31 magnesium alloy, Mater. Sci. Eng., A 543 (2012) 200–209.

[16] C.D. Allen, W.J. Arbegast, Evaluation of friction spot welds in aluminum alloys, SAE International, 2005. pp. 107–13.

[17] A. Patnaik, K. Koch, W.J. Arbegast, C.D. Allen, Static properties of refill friction spot welded skin stiffened compression panels, SAE technical paper 2006–01-0967. Warrendale, USA: SAE International.

[18] S.L. Fox, Refill friction spot weld repair of a fatigue crack, Research Experience for Undergraduates, South Dakota School of Mines and Technology, Rapid City (USA), 2010.

[19] C. Schilling, J. dos Santos, Method and device for joining at least two adjoining work pieces by friction welding, International Patent Publication. United States Patent 6722556. International Patent Publication: Google Patents, 2004.

[20] S.T. Amancio-Filho, A.P.C. Camillo, L. Bergmann, J.F. Dos Santos, S.E. Kury, N.G.A. Machado, Preliminary investigation of the microstructure and mechanical behaviour of 2024 aluminium alloy friction spot welds, Mater. Trans. 52 (2011) 985–991.

[21] Y.S. Sato, M. Urata, H. Kokawa, Parameters controlling microstructure and hardness during friction-stir welding of precipitation-hardenable aluminum alloy 6063, Metall. Mater. Trans. A 33 (2002) 625–635.

[22] Y. Lin, Z.Q. Zheng, Y. Han, H.F. Zhang, Effects of heat treatment process on tensile and corrosion properties of 2A97 Al–Li alloy, Trans. Nonferr. Metal. Soc. (2012) 2181–2186.

[23] C. Gao, Y. Luan, J.C. Yu, Y. Ma, Effect of thermo-mechanical treatment process on microstructure and mechanical properties of 2A97 Al–Li alloy, Trans. Nonferr. Metal. Soc. 24 (2014) 2196–2202.

[24] Q.Y. Shi, X.B. Wang, X. Kang, Y.J. Sun, Temperature fields during friction stir welding, J. Tsinghua Univ. (2010) 980-3+8.

[25] P. Prangnell, C. Heason, Grain structure formation during friction stir welding observed by the 'stop action technique', Acta Mater. 53 (2005) 3179–3192.

[26] H.L. Hao, D.R. Ni, Z. Zhang, D. Wang, B.L. Xiao, Z.Y. Ma, Microstructure and mechanical properties of Al–Mg–Er sheets jointed by friction stir welding, Mater. Des. 52 (2013) 706–712.

[27] L.H. Wu, D. Wang, B.L. Xiao, Z.Y. Ma, Microstructural evolution of the thermomechanically affected zone in a Ti–6Al–4V friction stir welded joint, Scripta Mater. 78–79 (2014) 17–20.

[28] P. Campestrini, H. Terryn, A. Hovestad, J. De Wit, Formation of a cerium-based conversion coating on AA2024: relationship with the microstructure, Surf. Coat. Technol. 176 (2004) 365–381.

[29] D. Tsivoulas, J.D. Robson, C. Sigli, P.B. Prangnell, Interactions between zirconium and manganese dispersoid-forming elements on their combined addition in Al–Cu–Li alloys, Acta Mater. 60 (2012) 5245–5259.

[30] A. Shukla, W. Baeslack III, Study of microstructural evolution in friction-stir welded thin-sheet Al–Cu–Li alloy using transmission-electron microscopy, Scripta Mater. 56 (2007) 513–516.

[31] C. Giummarra, B. Thomas, R.J. Rioja, New aluminum lithium alloys for aerospace applications, in: Proceedings of the light metals technology conference, Ottawa, Canada, 2007, pp. 24–6.

[32] B. Gault, X.Y. Cui, M.P. Moody, F. De Geuser, C. Sigli, S.P. Ringer, et al., Atom probe microscopy investigation of Mg site occupancy within δ' precipitates in an Al–Mg–Li alloy, Scripta Mater. 66 (2012) 903–906.

[33] L.A.H. Terrones, S.N. Monteiro, Composite precipitates in a commercial Al–Li–Cu–Mg–Zr alloy, Mater. Charact. 58 (2007) 156–161.

[34] W. Cassada, G. Shiflet, E. Starke, Mechanism of Al2CuLi (T1) nucleation and growth, Metall. Trans. A 22 (1991) 287–297.

[35] H.J. Kim, M. Niinomi, The role of microstructures on the strengthening mechanisms of a thermomechanically processed 2091 Al–Li alloy, Mater. Sci. Eng., A 284 (2000) 14–24.

[36] Y. Lin, Z.Q. Zheng, H.F. Zhang, Y. Han, Effect of heat treatment process on tensile properties of 2A97 Al–Li alloy: experiment and BP neural network simulation, Trans. Nonferr. Metal. Soc. 23 (2013) 1728–1736.

[37] O. Myhr, Ø. Grong, S. Klokkehaug, H. Fjoer, A. Kluken, Process model for welding of Al–Mg–Si extrusions Part 1: precipitate stability, Sci. Technol. Weld. Join. 2 (1997) 245–253.

[38] D. Kuhlmann-Wilsdorf, Theory of plastic deformation: properties of low energy dislocation structures, Mater. Sci. Eng., A 113 (1989) 1–41.

[39] P. Donnadieu, Y. Shao, F. De Geuser, G.A. Botton, S. Lazar, M. Cheynet, et al., Atomic structure of T1 precipitates in Al–Li–Cu alloys revisited with HAADF-STEM imaging and small-angle X-ray scattering, Acta Mater. 59 (2011) 462–472.

[40] S. Ahmadi, H. Arabi, A. Shokuhfar, Formation mechanisms of precipitates in an Al–Cu–Li–Zr alloy and their effects on strength and electrical resistance of the alloy, J. Alloys Compd. 484 (2009) 90–94.

[41] F.W. Gayle, F.H. Heubaum, J.R. Pickens, Structure and properties during aging of an ultra-high strength Al–Cu–Li–Ag–Mg alloy, Scripta Metall. Mater. 24 (1990) 79–84.

[42] X.M. Zhang, Y.W. Liu, L.Y. Ye, J.G. Tang, Effects of pre-deformation on precipitating behavior and grain refinement of AA2195 Al–Li alloy, J. Cent. South Univ. (2009) 375–382.

[43] L.H. An, Y. Cai, W. Liu, S.J. Yuan, S.Q. Zhu, F.C. Meng, Effect of pre-deformation on microstructure and mechanical properties of 2219 aluminum alloy sheet by thermomechanical treatment, Trans. Nonferr. Metal. Soc. 22 (2012). s370-s5.